JOURNAL OF APPLIED ELECTROCHEMISTRY 19 (1989) 505–511

The distribution of voltage losses among components of a battery

HIRAM GU

Physical Chemistry Department, General Motors Research Laboratories, Warren, Michigan 49090-9055, USA

Received 4 June 1988; revised 4 October 1988

An approach to identify the contribution of each individual component to the total voltage loss of a battery is presented. This approach combines experimental measurements with a mathematical model of the grid geometry to assess voltage losses due to: (a) terminal post; (b) intercell connector; (c) separator; (d) positive and negative electrodes; (e) positive and negative grids. A circuit model is used to relate the component resistances to the resistance of the battery. The versatile grid geometry model also allows one to predict the effect of a grid design change to the overall performance of a battery.

1. Introduction

The maximum theoretical power of a battery is its equilibrium terminal voltage multiplied by the discharge current. The actual power available from a battery, however, is always less because of electrode kinetics, mass transfer and ohmic losses. In order to minimize these losses, it is important to know the relative contribution of each component of a battery to the total voltage loss. Possible improvements in the performance of a battery can be assessed if the critical components contributing to the losses can be identified. It is also important to be able to predict the performance improvement from a design change – minimizing the need for build-and-test – to reduce development cost.

In this paper, a mathematical model to evaluate grid geometry is presented. This model is a resistive network model that predicts the voltage difference between the positive plate lug and the negative plate lug with the applied current used as an input parameter. The effective resistance of the positive and negative grids (current collectors) can be determined with the help of this model.

Tiedemann *et al.* [1] reported a resistive network model of an unpasted lead–acid battery grid. They assumed a uniform current density on the face of the plate and examined the potential distribution on the grid. Vaaler *et al.* [2] modeled both positive and negative plates simultaneously without the restriction of uniform current density. Linear polarization resistance was used between the plates. Subsequently, Tiedemann and Newman [3] expanded their earlier model to: (a) eliminate the restriction of uniform current density; (b) include time dependency; (c) consider both linear and nonlinear polarizations. Their model was applicable to a cell with grid junctions of the positive and negative grids that are directly aligned. Gu [4] reported a model to analyze the nickel–zinc battery with expanded metal grids. The model included time dependency as well as linear and nonlinear polarization features but was limited to analyzing a grid geometry with repetitive patterns that can be substituted by an equivalent geometry with rectilinear grid elements.

Sunu and Burrows [5] were the first to examine a grid geometry with two non-rectilinear grid elements in the lead dioxide plate. The two elements were assumed to conduct current in the plane of the electrode but do not contain nodes that collect current flowing between the positive and negative plates. Furthermore, only junctions between the diagonal and horizontal elements – not the vertical elements – were considered as nodes in the model. They also assumed uniform current density over the plate. Subsequently, they eliminated the requirement for uniform current distribution and iterated on the distribution of the current density to determine convergence in their model calculations [6]. In their model, an imaginary node (mathematical node) is used on the positive plate for each grid junction (physical node) on the negative plate if no counter junction exists on the positive plate. This approach taken by Sunu and Burrows requires tedious set-up procedures and may not be suitable for computer-aided design applications, especially if more non-rectilinear elements are involved.

Recently, Morimoto *et al.* [7] presented a model that includes dependencies of active material resistivity, electrolyte concentration and voltage–current relationship on the state of charge. The grids that they can evaluate, however, are still limited to those with a rectilinear geometry.

The approach used in the present grid geometry model allows handling of a large number of non-rectilinear grid elements on either grid. The transformation to the resistive network is simple and direct. By combining experimental measurements with this

0021-891X/89 $03.00 + .12

flexible mathematical model, one can quickly determine the voltage loss due to each component: (a) terminal post; (b) intercell connector; (c) separator; (d) positive and negative electrodes (paste); (e) positive and negative grids. A circuit analog model is used to relate the component resistances to the battery resistance. The grid geometry model also allows one to predict improvements from changes in grid design.

An overview of this systematic approach to identify voltage losses has previously been reported [8]. This paper gives an in-depth description of the approach and the grid geometry model, applied to a lead–acid battery. The assessment of the voltage losses is based on the initial state of discharge, during which the electrolyte concentration is relatively uniform.

2. Details of approach

The procedures used in this systematic approach include: (a) classical measurements of the terminal and connector resistances, the separator resistance and electrode polarizations; (b) application of the mathematical model relating to the grid geometry; (c) assessment of component contributions to the voltage loss of the battery based on a circuit analog model.

The terminal post resistance (R_t) and the intercell connector resistance (R_{ic}) can be measured, e.g. at room temperature using a 4-terminal milliohmmeter such as the Hewlett–Packard 4328A. For the lead–acid battery examined in this work, the terminal post and the intercell connector have about the same resistance of 0.1 mΩ. Within the operable temperature range of the battery, the resistance at another temperature can be calculated from an approximately linear relationship [9], e.g. the resistance for lead at $-18°$ C is about 83% of that at room temperature.

The separator resistance as a function of temperature can be measured using a fixture first reported by Lander and Weaver [10] with the 4-terminal milliohmmeter. In our version of the fixture (Fig. 1), there are two movable blocks between which the separator is placed. Each block has a compartment for the voltage probe and a capillary that extends to a 1-cm^2 hole, where the current passes through the sample. The fixture is filled with the electrolyte of interest, e.g. 1.280 specific gravity sulfuric acid. When the movable blocks are pressed together without the separator, a cell constant, due to the gap between the capillary tips, is measured. The difference between the resistance measured with the separator and the cell constant is the true resistance of the separator. Since the cross-sectional area of the current path is 1 cm^2, the resistance measured is also the area-independent resistance of the separator in Ω cm^2.

An Arrhenius-type relationship can be used to express the temperature dependence of the separator resistance.

$$r_s = r_0 \exp\left[B\left(\frac{1}{T} - \frac{1}{T_0}\right)\right] \quad (1)$$

where r_s is the separator resistance (Ω cm^2) at the temperature T(K), r_0 is the separator resistance at the temperature T_0, and B(K^{-1}) is a constant related to the excitation energy of the conduction process. By measuring the separator resistance as a function of temperature, the constant B and the resistance r_0 at the reference temperature, e.g. 0° C (T_0 = 273.15 K) are determined from a non-linear regression fit of the data obtained at different temperatures (Fig. 2).

Figure 2 gives three sets of resistance data obtained in 5 mol dm^{-3} sulfuric acid, using two separators. Three sets of measurements were made to account for variability in the separator, and two separators were used to improve accuracy because of the large cell constant of our cell. The separator resistance and the cell constant are plotted in Fig. 3. The cell constant is more than double the separator resistance. The data of Fig. 3 give r_0 (at 0° C) = 0.26 Ω cm^2 and $B = 1.8 \times 10^3$ K^{-1}.

There are two approaches to determine the combined voltage loss due to the positive and negative

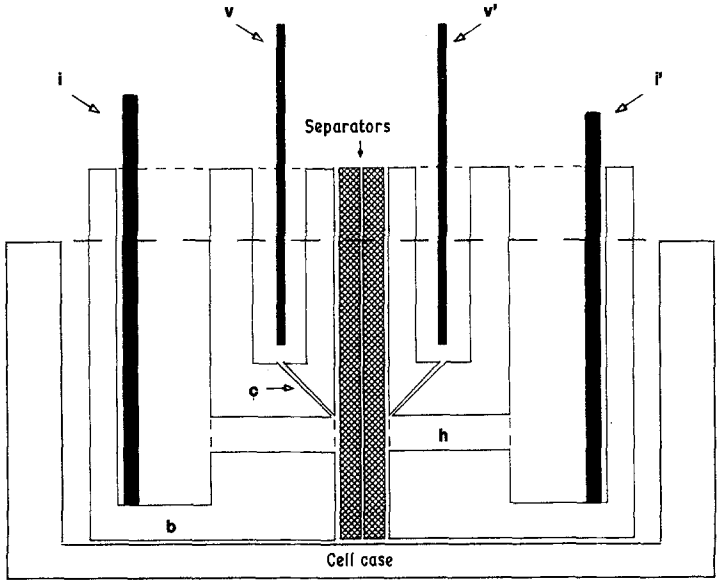

Fig. 1. A schematic of the fixture used to measure separator resistance. v, v', voltage probe connections; i, i', current probe connections; h, 1-cm^2 hole; b, movable block; c, capillary.

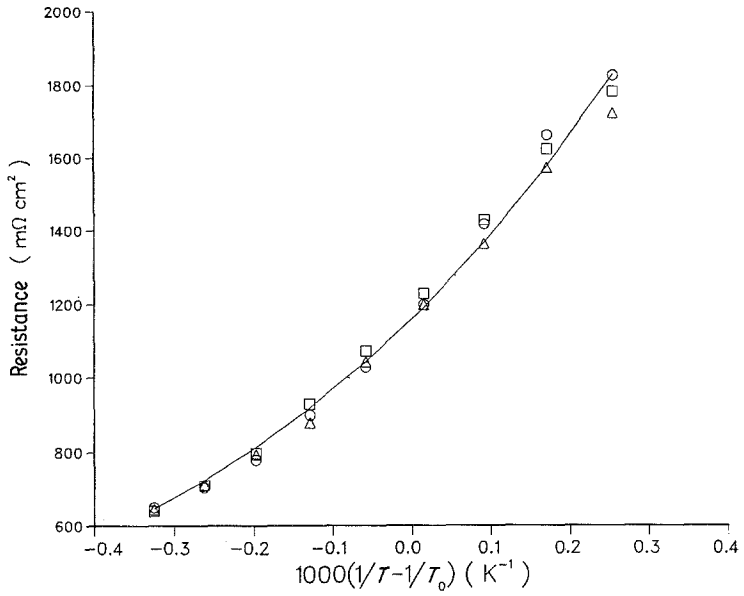

Fig. 2. Resistance data with two separators. The three sets of data are identified by different symbols. The regression fit is shown as the solid curve.

electrodes. In the first approach, a mathematical model of the cell chemistry – electrode kinetics, material conservation and transport phenomena – can be used to calculate the cell voltage [11]. The voltage losses due to each electrode as well as the separator can be obtained from this model. This mathematical model is a useful tool to evaluate cell designs such as electrode thickness, electrode porosity and separator characteristics, but it requires knowledge of the fundamental parameters that appear in the formulation. If the objective is mainly an assessment of the contribution of each component to the total voltage loss of the battery, it is more effective to take another approach – use an empirical model. To obtain data for the empirical model, a small experimental cell shown in Fig. 4 is used [4]. The apparent area of the plates used in the cell is typically about 5 cm^2, which is a few per cent of a full-size plate. By using small plates, the ohmic losses of the grids can be neglected and a relatively uniform current distribution is obtained. For the lead–acid cell, it has been found that the voltage–current relationship can be adequately expressed by a linear empirical model:

$$i = Y(\phi_p - \phi_n - U) \quad (2)$$

where i is the applied current density (A cm^{-2}), U is the equilibrium cell potential (V), Y is the reciprocal of the slope (S cm^{-2}), and $\phi_p - \phi_n$ is the measured cell voltage. Y is a function of the state of charge and so is U since the acid concentration in the cell is changing. But for the purpose of identifying the relative contribution of each component, it is reasonable to restrict ourselves to the initial state of discharge when all the variables are still relatively constant. The combined electrode resistance (r_e) can be obtained after the separator contribution is subtracted.

Figure 5 gives the initial voltage loss from U(2.1 V) as a function of the current density, with the ambient temperature at −18° C. Within the range shown, the slope of the line is 1.34 Ω cm^2, which is Y^{-1} at the fully charged state. The separator resistance (r_s) at −18° C according to Equation 1 is 0.41 Ω cm^2, hence r_e = 0.93 Ω cm^2.

The grid geometry model is used to determine the

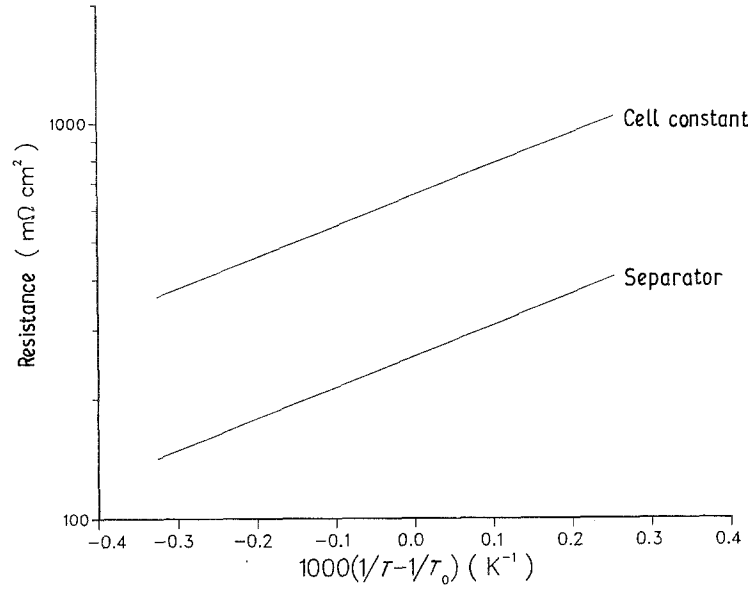

Fig. 3. The separator resistance and the cell constant with 5 mol dm^{-3} sulfuric acid.

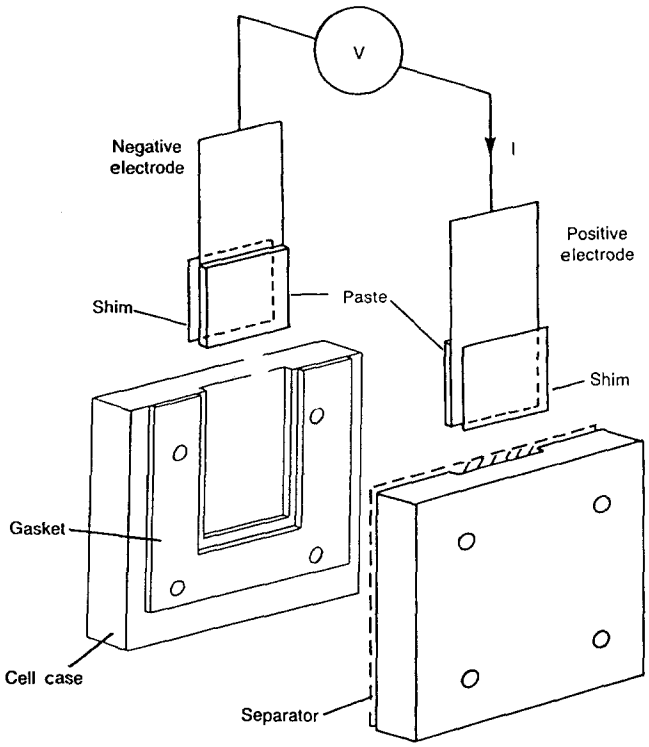

Fig. 4. A small experimental cell to determine cell polarization without the influence of grid ohmic losses.

contribution of the grids to the total loss of the battery. In the model, the grid is transformed into a network of resistors. The concept is straightforward, but the difficulty has been to find a simple way to set up the nodes (physical or mathematical) on two electrode plates, especially with intricate grid designs. The present approach eliminates this difficulty by creating a uniform set of $n \times n$ nodes (or $n \times m$) with equal spacings in both directions. For a node on the negative plate, there is always a matching node on the positive plate. The total number of nodes used in the model is $2n^2$ (or $2nm$).

If we use x as the index for the horizontal direction, and y as the index for the vertical direction, Kirchoff's law applied to node (x, y) is:

$$\frac{\phi_{x+1,y} - \phi_{x,y}}{R^h_{x+1,y}} + \frac{\phi_{x-1,y} - \phi_{x,y}}{R^h_{x,y}} + \frac{\phi_{x,y+1} - \phi_{x,y}}{R^v_{x,y+1}} + \frac{\phi_{x,y-1} - \phi_{x,y}}{R^v_{x,y}} + i_{xy}A_{x,y} = 0 \qquad (3)$$

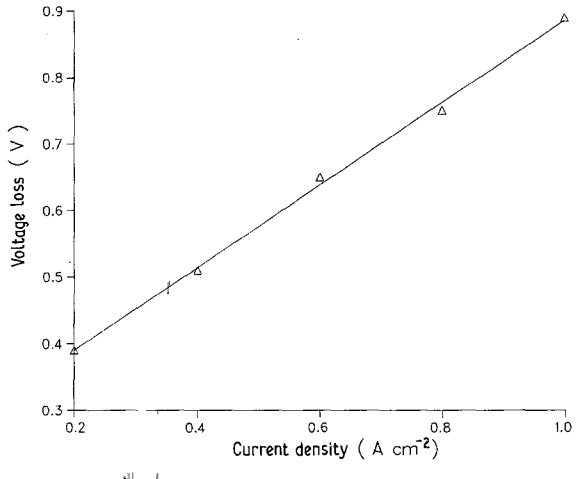

Fig. 5. Initial voltage drop as a function of the current density obtained from small experimental cells.

where $\phi_{i,j}$ are potentials in volt, $R^h_{i,j}$ are effective resistances in Ω between nodes in the x direction and $R^v_{i,j}$ are for those in the y direction, $i_{x,y}$ is the current density at (x, y) in A cm^{-2}, and $A_{x,y}$ is the area associated with the node in cm^2. The empirical polarization model (Equation 2) is used to relate $i_{x,y}$ to the difference between $\phi^p_{x,y}$ on the positive plate and $\phi^n_{x,y}$ on the negative plate.

For two nodes on a plate with no connecting grid element, the resistance between the nodes is calculated from the resistivity of the electrode paste (active material). If a grid element is present, the effective resistance is the parallel combination of the grid resistance and the paste.

A diagonal grid element is approximated by segments of vertical and horizontal elements that pass through established nodes, resembling a staircase. The

Table 1. Parameters used in the sample calculations

Applied current	= 405 A
Ambient temperature	= −18° C
Number of positive plates	= 4
Number of negative plates	= 5
Plate width	= 13.90 cm
Plate height	= 10.70 cm
Grid top border	
cross-sectional area	= 0.028 cm^2
resistivity	= 2.06 × 10^{-5} Ω cm
Grid elements	
cross-sectional area	= 0.007 cm^2
resistivity	= 2.06 × 10^{-5} Ω cm
Grid lug resistance	= 3.18 × 10^{-4} Ω
Paste resistivity	
positive electrode	= 0.01 Ω cm cm^{-1}
negative electrode	= 0.001 Ω cm cm^{-1}
U	= 2.1 V
Y^{-1}	= 1.34 Ω cm^2

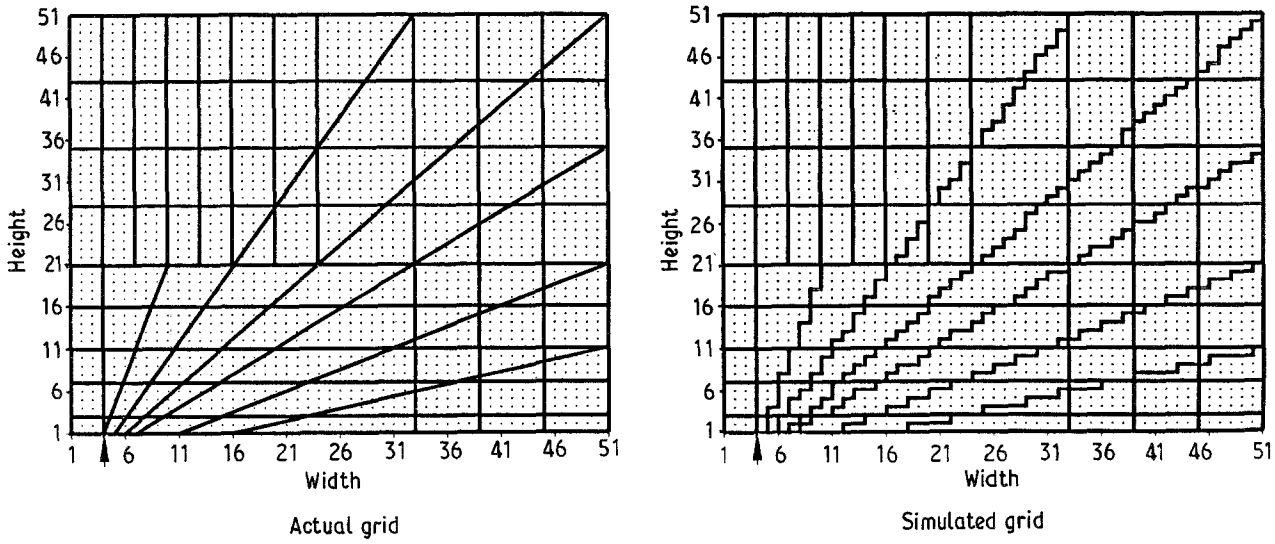

Fig. 6. Model simulation of an actual grid.

resistance of the simulated grid element is adjusted (reduced) relative to the real grid element to account for the increased length of the simulated element. An example of the simulated grid layout is shown in Fig. 6 together with the actual grid pattern as generated by the computer. The arrowhead indicates the location of the grid lug, which is at the top border of the grid. The grid can be visualized as laying flat on the page with the lug pointing toward the reader.

Using the grid pattern shown in Fig. 6 as an example case: (a) the usefulness of the model to evaluate grid geometry will be demonstrated; (b) the effective resistances for a grid with the intricate pattern and one with a rectilinear pattern will be calculated; (c) comparison will be made between the two patterns. The parameters used in the calculations are summarized in Table 1.

Only one grid is shown in Fig. 6 with the lug located at (4, 1). The other grid is a mirror image with the lug located at (48, 1). The calculated initial cell voltage under the 405 A discharge is 1.268 V – a loss of 0.832 V from the open-circuit voltage. The equivalent resistance of the cell is thus 2.05 mΩ (R_c) or 2.44 Ω cm^2 (r_c) since the current density is 0.34 A cm^{-2}. The effective grid resistance (r_g^{eff}) is 1.10 Ω cm^2 after the resistance due to the electrodes and the separator (1.34 Ω cm^2) is subtracted. The total length of the elements of each grid in this case is 312 cm. We will designate the geometry shown in Fig. 6 the grid-A design.

Next, we will consider a grid pattern shown in Fig. 7 for both positive and negative plates (grid-B design) with the lugs located at (4, 1) and (48, 1), respectively. More vertical grid elements have been placed at the top half portion of the grid (near the lug) to improve conductivity. The total length of the elements per grid is 401 cm, about 28% greater than grid A. The calculated cell voltage is 1.241 V – a loss of 0.859 V that is 3% greater than the grid-A design. The effective grid resistance is 1.19 Ω cm^2, which is 8% more than the grid-A design.

The grid-A design has the advantages of being lighter in weight (shorter total element length) and lower in resistance than the grid-B design. However, there are open areas in the grid-A design that may require light-weight support elements to hold the

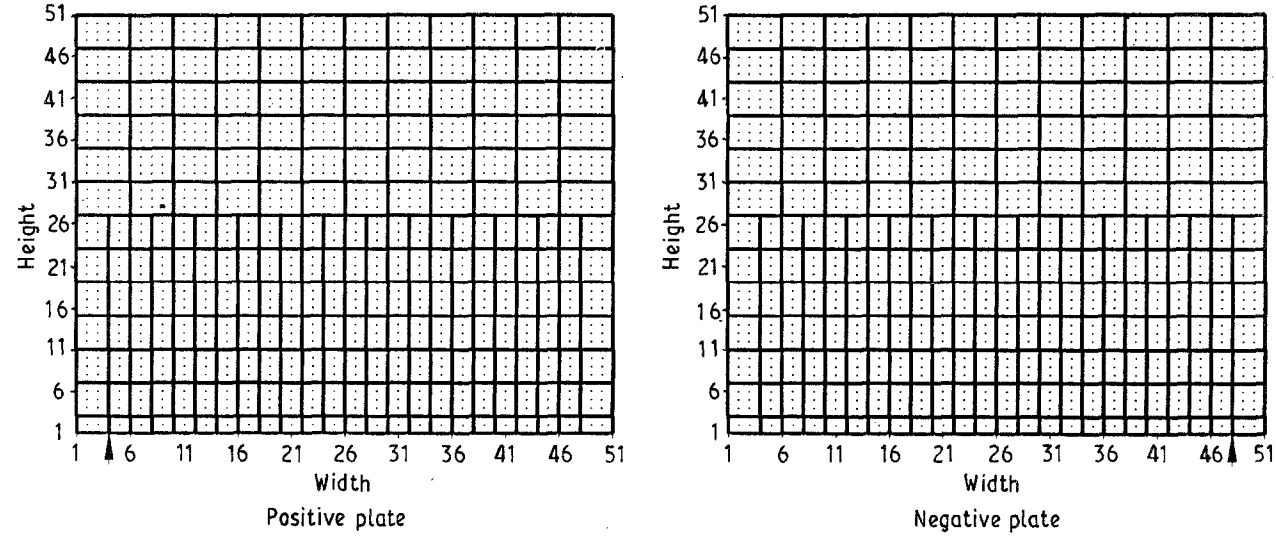

Fig. 7. A rectilinear grid geometry layout.

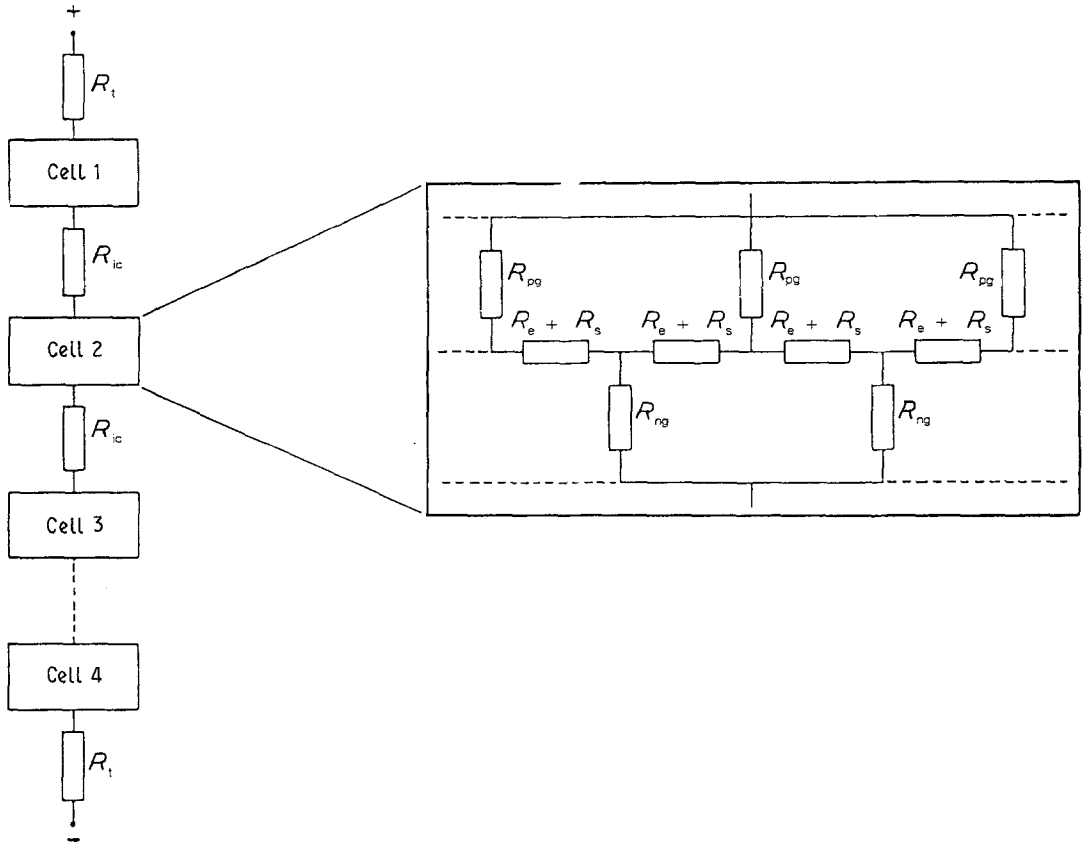

Fig. 8. A circuit analog of a battery.

active material in place. If so, its benefit in weight (material) reduction will be reduced.

We have so far considered only the combined effective grid resistance. The grid geometry model can also be used to estimate the effective resistance of each grid – positive or negative. The effective resistance of a grid is estimated by applying the model with the other grid assumed to be highly conductive. The sum of the two estimated effective resistances (positive and negative), however, will not be exactly equal to the combined effective resistance because the current distributions for the three cases are all different.

The grid geometry model has taken into account the nonuniform distribution of current between the plates and provides one with an effective grid resistance. A simple circuit analog (Fig. 8) can now be used to relate the component resistances to the battery resistance. In Fig. 8, R_{pg} represents the positive grid resistance (Ω), R_{ng} is the negative grid resistance, R_e is the electrode resistance that is equal to r_e/A (A being the apparent plate area, 13.90 cm × 10.70 cm), and R_s is the separator resistance that is equal to r_s/A.

A closed-form solution can be obtained for the circuit shown in Fig. 8 if we assume the outside plates of a cell pack have grids that are twice the resistance of the grids of the inside plates. This is a good assumption because the outside plates – used as half electrodes – are asked to carry only half of the current that an inside plate has to carry. Therefore, in principle, the grids of the outside plates should be designed to have twice the resistance as the grids in the inside plates for the same voltage loss – although this is never done due to cost. For a cell with n plates and a battery with N cells connected in series, the battery resistance R_b is:

$$\begin{aligned} R_b &= 2R_t + (N-1)R_{ic} + NR_c \\ &= 2R_t + (N-1)R_{ic} + \frac{2N}{n-1}(R_{pg} + R_{ng}) \\ &\quad + \frac{N}{n-1}(R_e + R_s) \end{aligned} \tag{4}$$

Contributions of the components to the voltage losses of the two batteries – one with grid A and one with grid B – are shown in Fig. 9. Although the battery with grid A uses 28% less grid material than the one with grid B, it still demonstrates a 2% improvement in performance over the one with grid B. For both batteries, over 40% of the losses are from the grids. The losses in the electrodes are also significant at −18° C. Both electrode and separator losses will decrease close to an exponential fashion with an increase in ambient temperature while the losses due to the grids will rise slightly since the resistivity of lead will increase with temperature. In view of the significant contribution of the grids to the voltage loss of the battery, more improvements in the grid geometry will, no doubt, be beneficial.

The work presented has been focused on accessing the relative contribution of each component to the total voltage loss of a battery at the initial state of discharge. The approach employed, however, is not restrictive to the initial state of discharge as long as time-dependent data is collected, such as those presented by Gu [4] and Morimoto *et al.* [7].

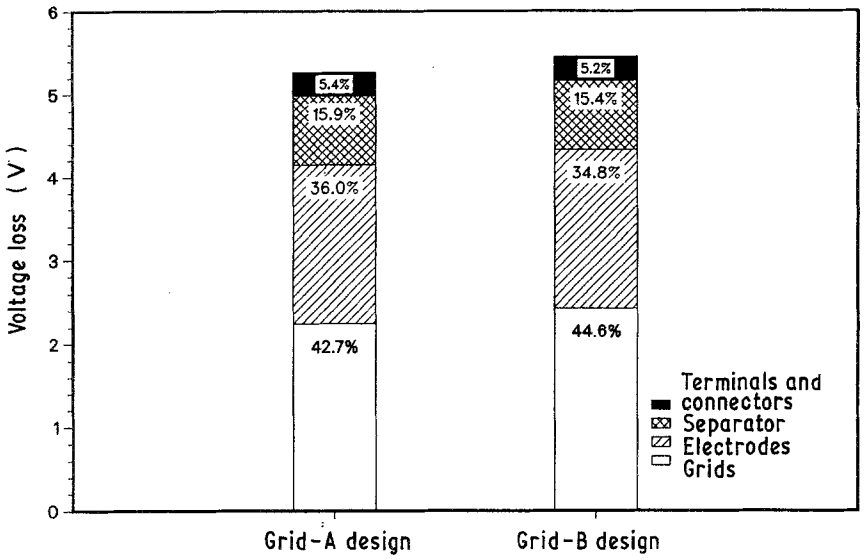

Fig. 9. Various voltage losses in the lead-acid batteries under a 405 A load at −18° C.

3. Conclusions

By combining simple classical measurements and experiments with a resistive network model of the grid geometry, we are able to identify critical components limiting battery performance, thus providing guidelines for development focuses. Also, as a result of using the staircase approximation in the grid geometry model, very little set-up time is required to make a calculation. Hence, a new grid design can be evaluated quickly.

Acknowledgement

The author acknowledges the support of the Delco-Remy Division of General Motors.

References

[1] W. H. Tiedemann, J. Newman and F. Desua, in 'Power Sources 6' (edited by D. H. Collins), Academic Press, New York (1977) p.15.

[2] L. E. Vaaler, E. W. Brooman and H. A. Fuggiti, *J. Appl. Electrochem.* **12** (1982) 721.

[3] W. H. Tiedemann and J. Newman, in 'Battery Design and Optimization' (edited by S. Gross), The Electrochemical Society Softbound Proceedings Series, Princeton, NJ (1979) p. 23.

[4] H. Gu, *J. Electrochem. Soc.* **130** (1982) 1459.

[5] W. G. Sunu and B. W. Burrows, *J. Electrochem. Soc.* **129** (1982) 688.

[6] W. G. Sunu and B. W. Burrows, *J. Electrochem. Soc.* **131** (1984) 1.

[7] Y. Morimoto, Y. Ohya, K. Abe, T. Yoshido and H. Morimoto, *J. Electrochem. Soc.* **135** (1988) 293.

[8] H. Gu, R. L. Galyen and G. W. Brutchen, in 'Electrochemical Engineering Applications' (edited by R. E. White, R. F. Savinell and A. Schneider), AIChE Symposium Series No. 254, Vol. 83 (1987) p. 92.

[9] R. H. Perry, C. H. Chilton and S. D. Kirkpatrick, 'Perry's Chemical Engineers' Handbook', 4th edn, McGraw-Hill, Chichester (1963) p. 25-3.

[10] J. J. Lander and R. D. Weaver, in 'Characteristics of Separators for Alkaline Silver Oxide Zinc Secondary Batteries (edited by J. E. Cooper and A. Fleischer), AD 447301 U.S. Air Force Manual (1964) Chap. 6a.

[11] H. Gu, T. V. Nguyen and R. F. White, *J. Electrochem. Soc.* **134** (1987) 2953.